Heliyon 10 (2024) e34596

Contents lists available at ScienceDirect

Heliyon

journal homepage: www.cell.com/heliyon

Research article

A classic prescription alleviates inflammation in CUMS model mice via modulating MYDGF/MAP4K4/NF-κB signaling pathway, verified through UPLC-HRMS and proteomics analysis

Ruolan Huang [a,b], Shenglan Gong [c,d], Bocheng Xiong [e], Xifei Yang [e], Chongyang Chen [f], Wei Song [a], Ruodai Wu [b], Li Yang [b], Jia Yin [a,**], Mingtai Chen [g,h,*]

[a] Nanfang Hospital, Southern Medical University, Guangzhou, Guangdong, China
[b] Shenzhen University General Hospital, Clinical Research Center for Neurological Diseases, Shenzhen University, Shenzhen, Guangdong, China
[c] Department of Cardiovascular Disease, Shenzhen Hospital (Futian) of Guangzhou University of Chinese Medicine, Shenzhen, Guangdong, China
[d] Sixth Clinical Medical College, Guangzhou University of Chinese Medicine, Shenzhen, Guangdong, China
[e] Shenzhen Key Laboratory of Modern Toxicology, Shenzhen Medical Key Discipline of Health Toxicology (2020-2024), Shenzhen Center for Disease Control and Prevention, Shenzhen, Guangdong, China
[f] Key Laboratory of Nuclear Medicine, Ministry of Health, Jiangsu Key Laboratory of Molecular Nuclear Medicine, Jiangsu Institute of Nuclear Medicine, Wuxi, Jiangsu, China
[g] Shenzhen Traditional Chinese Medicine Hospital, Guangzhou University of Chinese Medicine, Shenzhen, Guangdong, China
[h] Faculty of Chinese Medicine and State Key Laboratory of Quality Research in Chinese Medicine, Macau University of Science and Technology, Taipa, Macao, China

ARTICLE INFO

Keywords:
Major depressive disorder
Chronic unpredictable mild stress
Inflammation
Herbal medicine
MYDGF

ABSTRACT

Background: Xiaoyaosan (XYS), a renowned classical traditional Chinese medicinal formula utilized in addressing major depressive disorder (MDD), has garnered significant acclaim for its remarkable efficacy in clinical application. The onset of major depressive disorder (MDD) often correlates with chronic unpredictable mild stress (CUMS), a pivotal instigating factor in its development.

Aim of the study: This study aims to clarify the potential anti-inflammatory mechanisms of XYS in treating CUMS model mice.

Materials and methods: Utilizing cutting-edge ultra high-performance liquid chromatography - high-resolution mass spectrometry (UPLC-HRMS), the active constituents of XYS were discerned, while employing proteomics analysis to delve into the potential mechanisms of its efficacy. Molecular docking studies, alongside subsequent *in vivo* experiments utilizing CUMS model mice, were conducted to corroborate the findings derived from the proteomics analysis.

Results: In vivo experiments demonstrated that XYS not only markedly ameliorated behavioral markers but also attenuated serum inflammatory markers and suppressed IL-6 and TNF-α expression within the brains of CUMS model mice. Proteomics analysis suggested that the pivotal anti-inflammatory mechanism of XYS against CUMS-induced damage might involve modulation

* Corresponding author. Shenzhen Traditional Chinese Medicine Hospital, Guangzhou University of Chinese Medicine, No.1 Fuhua Road, Futian District, Shenzhen, Guangdong, China.

** Corresponding author. Department of Neurology, Nanfang Hospital, Southern Medical University, Guangzhou, Address No. 1023, South Shatai Road, Baiyun District, Guangzhou, Guangdong, China.

E-mail addresses: yinj@smu.edu.cn (J. Yin), zyycardio@foxmail.com (M. Chen).

https://doi.org/10.1016/j.heliyon.2024.e34596
Received 8 March 2024; Received in revised form 24 June 2024; Accepted 12 July 2024
Available online 14 July 2024

of the MAPK signaling pathway. Utilizing UPLC-HRMS, the active constituents of XYS were successfully identified, while molecular docking investigations explored interactions between XYS and MYDGF, PKC, MAP4K4, P-p65, p65, P-IKBα, and IKBα. The findings revealed XYS's regulatory influence on the MYDGF/MAP4K4/NF-κB signaling cascade.

Conclusions: This study is the first to our knowledge to demonstrate that XYS can alleviate inflammation in CUMS model mice by modulating the MYDGF/MAP4K4/NF-κB signaling pathway.

Abbreviations

BH	Bohe
BS	Baishao
BZ	Baizhu
CH	Chaihu
CUMS	Chronic unpredictable mild stress
DG	Danggui
FL	Fuling
GC	Gancao
GJ	Ganjiang
GO	Gene Ontology
GR	glucocorticoid receptors
HPA	hypothalamic-pituitary-adrenal
IFN-γ	interferon-γ
IL-1β	interleukin-1β
KEGG	Kyoto Encyclopedia of Genes and Genomes
MAP4K4	mitogen-activated protein kinase kinase kinase kinase 4
MAPK	mitogen-activated protein kinase
MDD	Major depressive disorder
MYDGF	myeloid cell–specific myeloid-derived growth factor
NLRP3	NOD-like receptors family pyrin domain containing 3
OFT	open field test
p65	nuclear factor NF-kappa-B p105 subunit
PKC	protein kinase C
SSRIs	Selective serotonin reuptake inhibitors
TCM	traditional Chinese medicine
TNF-α	tumor necrosis factor-α
UPLC-HRMS	Ultra high performance liquid chromatography - High resolution mass spectrometry
WHO	World Health Organization
XYS	Xiaoyaosan.

1. Introduction

Major depressive disorder (MDD) stands as a formidable mental health adversary, characterized by enduring feelings of despair, reduced capacity for enjoyment, compromised decision-making abilities, and cognitive impairment, with a distressing escalation in suicide risk [1]. According to projections from the World Health Organization (WHO), the prevalence of depression is anticipated to affect over 350 million individuals worldwide by 2030, potentially emerging as the leading cause of disease burden [2]. Unfortunately, conventional antidepressant therapies face substantial challenges, including low response rates, prolonged treatment durations, and significant side effects, leading to resistance in up to 30 % of patients [3]. Selective serotonin reuptake inhibitors (SSRIs) remain the cornerstone of pharmacotherapy for MDD. However, research indicates nonresponse rates ranging from 30 % to 50 % among MDD patients to antidepressant interventions. Mounting evidence suggests that individuals with MDD often experience heightened stressors preceding onset, emphasizing chronic stress as a pivotal trigger for MDD. Chronic stress disrupts immune tolerance to glucocorticoids, leading to an imbalance in immune inflammation. Moreover, hyperactivation of the hypothalamic-pituitary-adrenal (HPA) axis and immune system results in reduced glucocorticoid receptor (GR) numbers and functionality, exacerbating the inflammatory cascade within the HPA axis [4–6].

Furthermore, certain MDD patients exhibit inflammatory responses devoid of physical illness, implicating inflammation in MDD pathogenesis [6–8]. Studies indicate elevated peripheral blood levels of interleukin-1β (IL-1β), IL-6, tumor necrosis factor-α (TNF-α),

interferon-γ (IFN-γ), chemokines, acute phase proteins, and adhesion molecules in MDD patients compared to healthy counterparts [6–8]. Given the bidirectional communication between peripheral blood and the central nervous system, peripheral inflammatory factors activate brain glial cells, initiating inflammatory cascades [8]. These findings underscore how chronic stress-induced HPA axis dysfunction and concomitant elevation of peripheral inflammatory factors exacerbate MDD pathophysiology, although the precise downstream mechanisms remain elusive.

Extensive clinical and preclinical investigations highlight the unique advantages of traditional Chinese medicine (TCM) in depression therapy, characterized by multitarget efficacy, significant therapeutic outcomes, and reduced adverse effects compared to many Western medications [9–15]. MDD falls within the TCM category of “Depression" (Yu Zheng), primarily attributed to “liver depression" and “spleen deficiency." Xiaoyaosan (XYS), a classical TCM formulation targeting liver depression and spleen deficiency, has amassed substantial clinical evidence demonstrating its efficacy against depression and harm induced by chronic unpredictable mild stress (CUMS) [9,10,12–15]. Derived from the classical TCM prescription “Taiping Huimin He Ji Ju Fang," XYS comprises eight herbs renowned for “liver soothing," depression alleviation, “blood nourishment," and “spleen strengthening." Current research

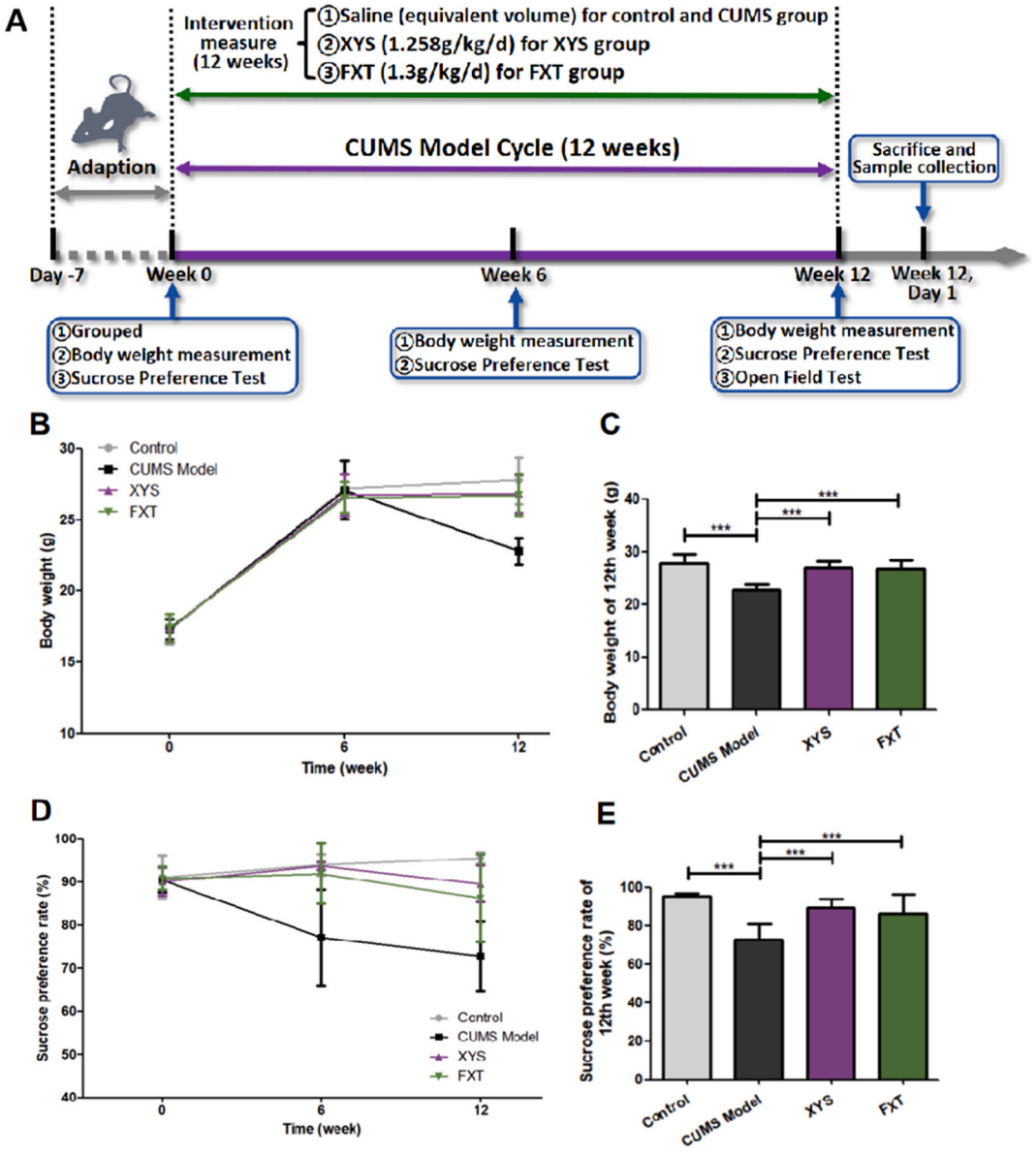

Fig. 1. Schedule of the experimental design and the effects of XYS on body weight and sucrose preference test of CUMS model mice. **(A)** Schedule of the experimental design. **(B)** The body weights of mice in each group at week 0, 6, and 12. **(C)** Bar graph of mice body weight in each group at week 12. **(D)** The sucrose preference test of mice in each group at week 0, 6, and 12. **(E)** Bar graph of mice sucrose preference test in each group at week 12. n.s, *, **, and *** represent not significant, $P < 0.05$, $P < 0.01$, and $P < 0.001$ respectively, in comparison with the CUMS model group.

elucidates various mechanisms underlying XYS's antidepressant effects. Studies report XYS's ability to alleviate depression-like symptoms and enhance synaptic survival and growth in CUMS-induced rats by suppressing the A2AR-ERK–NF–κB pathway [15]. Additionally, XYS mitigates core target genes implicated in necroptosis, enhances hippocampal function, and mitigates neuroinflammation in CUMS-induced mice [13]. Furthermore, XYS demonstrates antidepressant properties in CUMS-induced mice by potentially fostering hippocampal neurogenesis, reducing neuronal apoptosis, and restraining the overactivation of the IGF-1Rβ/PI3K/Akt pathway [14]. Nonetheless, research into XYS's mechanisms in ameliorating depression-like phenotypes by attenuating chronic inflammatory responses remains scarce. Hence, this study delves into XYS's anti-inflammatory mechanism in mitigating CUMS-induced injuries using an *in vivo* model.

The integration of proteomics, initially proposed by Wilkins et al. in the 1990s, into modern TCM research offers novel insights into diagnosing major diseases and developing innovative therapeutics [16]. Holism and syndrome differentiation, integral aspects of TCM, synergize with proteomics, providing novel perspectives on TCM interpretation and understanding [16–18]. Proteomic profiling serves as a vital tool in unraveling the intricate mechanisms underlying XYS's therapeutic effects by analyzing differentially expressed proteins and functional enrichment.

Finally, the identification of active compounds in TCM formulations remains paramount. Hence, this study employs ultra-high-performance liquid chromatography (UPLC) coupled with high-resolution mass spectrometry (HRMS) technology. UPLC facilitates rapid compound separation, while HRMS ensures exceptional selectivity, sensitivity, accuracy, and specificity [19,20]. This combined approach aids in structural speculation via secondary mass spectrometry, facilitating the identification of active compounds within XYS.

2. Materials and methods

2.1. Animals

Animal experiments were conducted adhering to the ARRIVE guidelines and with approval from the Local Ethical Committee (Guangzhou University of Chinese Medicine, Approval No. 20200817009). All C57BL/6 mice (males, 8 weeks old, Laboratory animal certificate No. 320730200100014676) were procured from Cavins Laboratory Animal Co. Ltd. of Changzhou (Changzhou, China) and individually housed in standard animal quarters (temperature: 22 ± 3 °C; humidity: 30–40 %; light cycle: 12 h/12 h dark/light) with ad libitum access to standard chow and water for acclimatization for at least one week.

2.2. CUMS model protocol and intervention

Following a one-week acclimation period, mice were randomly allocated into four groups: control, CUMS model, XYS (1.258 g/kg/d XYS granules), and FXT (1.3 g/kg/d fluoxetine tablet) serving as a positive control. Except for the control group, mice in the remaining groups underwent CUMS modeling for 12 weeks, following a protocol outlined in a previous study [21]. CUMS-induced mice were exposed to 1–2 unpredictable stressors daily, without repetition within three days, over a 12-week period. Stressors included flash stimulation, wet padding, restraint stress, empty cage exposure, water deprivation, cage tilt, new cage environment, fear stimulation, and nocturnal lighting. Details of the CUMS model and schedule are illustrated in Fig. 1A and Supplementary Table S1. To assess the impact of XYS and FXT on CUMS model mice, XYS (1.258 g/kg/d XYS granules) and FXT (1.3 g/kg/d fluoxetine tablet) were orally administered to mice in the respective treatment groups. Control and CUMS model group mice received equivalent volumes of saline daily throughout the CUMS modeling period until the study's conclusion. At the conclusion of the experiment, mice were fasted overnight, anesthetized, and euthanized. Serum and brain tissues were collected, sectioned, and preserved appropriately for subsequent analyses.

2.3. Identification of active compounds in XYS

XYS, a composite formulation of 8 natural herbal ingredients in granular form, embodies a harmonious blend of traditional Chinese medicinal elements. These components include Bupleuri Radix (Lot No. 0055491, Chinese name: Chaihu, CH, dried roots of *Bupleurum chinense DC.*), Angelicae Sinensis Radix (Lot No. 9129411, Chinese name: Danggui, DG, dried roots of *Angelica sinensis(Oliv.) Diels*), Paeoniae Radix Alba (Lot No. 0049441, Chinese name: Baishao, BS, dried roots of *Paeonia lactiflora Pall.*), Atractylodis Macrocephalae Rhizoma (Lot No. 0071791, Chinese name: Baizhu, BZ, dried rhizomes of *Atractylodes macrocephala Koidz.*), Poria (Lot No. 0071741, Chinese name: Fuling, FL, dried sclerotia of *Poria cocos (Schw.) Wolf*), Glycyrrhizae Radix Et Rhizoma (Lot No. 0059351, Chinese name: Gancao, GC, dried roots and rhizomes of *Glycyrrhiza uralensis Fisch.*), Menthae Haplocalycis Herba (Lot No. 0045621, Chinese name: Bohe, BH, dried aboveground parts of *Mentha haplocalyx Briq.*), and Zingiberis Rhizoma (Lot No. 0065291, Chinese name: Ganjiang, GJ, dried rhizomes of *Zingiber officinale Rosc.*). Each ingredient contributes distinct therapeutic properties to the formulation, with a balanced ratio of 2 : 2: 2 : 2: 2 : 1: 1 : 1, respectively. These meticulously selected herbs, provided by Guangdong Efong Pharmaceutical Co., Ltd. (China), are stored in separate airtight packages and dissolved in warm water before administration in the study to ensure their potency and efficacy. To identify the significant compounds present in XYS, ultra-performance liquid chromatography coupled with high-resolution mass spectrometry (UPLC-HRMS) was employed. This analysis, conducted by Shanghai Applied Protein Technology Co., Ltd., involved several meticulous steps. Initially, XYS granules were diluted with a 40 % methanol solution and subjected to centrifugation to isolate the supernatant. The resulting extract underwent thorough analysis using a Vanquish UPLC system equipped with an HSS-T3 column at a controlled temperature of 35 °C. The mobile phase, comprising water with 0.1 % formic acid (mobile phase

A) and acetonitrile with 0.1 % formic acid (mobile phase B), facilitated efficient separation of the compounds. LC-MS/MS analysis was then performed using a Thermo Q-Exactive HFX mass spectrometer in both positive and negative ionization modes. Data-dependent acquisition mode within a specified mass range (m/z 90–1300) enabled the acquisition of MS/MS spectra from the top 10 most intense MS1 ions. Sequential application of collision energies ensured accurate fragmentation of the compounds. The capillary temperature and probe heater temperature were carefully maintained throughout the analysis to optimize instrument performance and data quality. The annotation of the identified compounds was performed by matching accurate mass, isotopic distributions and MS/MS spectral to reference data from an in-house standards TCM database (Shanghai Applied ProteinTechnology CO., Ltd., Shanghai, China), which covers over 20,000 natural products spectra, including all Chinese herbal medicines in the Pharmacopoeia of the People's Republic of China. This comprehensive analytical approach facilitated the identification and characterization of the bioactive constituents present in XYS, shedding light on its pharmacological properties.

2.4. Sucrose preference test

Before initiating the test, mice were accommodated in cages and subjected to a 48-h sucrose solution adaptation period. During this time, two bottles of 1 % sucrose solution were provided for 24 h, followed by one bottle of 1 % sucrose solution and one bottle of regular water for another 24 h. Subsequently, mice underwent a 24-h period of food and water deprivation. Following deprivation, each mouse was placed individually in a cage equipped with two bottles: one containing 1 % sucrose solution and the other regular water. The positions of the bottles were alternated every 12 h. Mice were given unrestricted access to both solutions for 24 h, during which the consumption of each bottle was measured before and after the test. Sucrose preference was calculated using the formula: sucrose preference (%) = [sucrose solution intake (g)/(sucrose solution intake (g) + regular water intake (g))] × 100 %. Sucrose preference tests were conducted at weeks 0, 6, and 12.

2.5. Open field test

The mice were introduced to an open-field apparatus (100 × 100 × 40 cm) with a white background to carry out an open field test. In brief, the mice were placed in the middle of the box to adapt for 1 min and then allowed to explore for 5 min. Their behaviors were monitored using a camera (JL-Video Camera System, Shanghai Jiliang Software Science & Technology Co., Ltd), and the total distance traveled, average speed, time of activity, and time spent in the central area were calculated automatically for each mouse.

2.6. Enzyme-linked immunosorbent assay

The serum levels of corticosterone (CORT, Lot No. MM-0061M1, Jiangsu Meimian Industrial Co., Ltd, China), high-sensitivity C-reactive protein (hs-CRP, Lot No. MM-0372M1, Jiangsu Meimian Industrial Co., Ltd, China), lipoprotein-associated phospholipase A2 (Lp-PLA2, Lot No. MM-0474M1, Jiangsu Meimian Industrial Co., Ltd, China), Nuclear Factor Kappa B (NF-κB, Lot No. MM-44131M1, Jiangsu Meimian Industrial Co., Ltd, China), and Fibrinogen (FIB, Lot No. MM-0909M1, Jiangsu Meimian Industrial Co., Ltd, China) were detected using ELISA Kits according to the manufacturer's instructions. A Tecan Infinite M200 plate reader (Tecan, Durham, USA) was utilized to read the absorbance value of CORT, hs-CRP, Lp-PLA2, NF-κB, and FIB at 450 nm, and the serum levels of indicators above were calculated using Curve Expert software.

2.7. Proteomics analysis using liquid chromatography-mass spectrometry

Brain tissue samples from each mouse were meticulously collected and swiftly stored at −80 °C to preserve their integrity until further processing. Upon initiation of the experimental procedures, the tissues were submerged in a solution containing 8 M urea in PBS (pH 8.0). Sonication at low temperatures was then employed in the presence of protease and phosphatase inhibitors to facilitate tissue disruption. Following sonication, the samples underwent centrifugation at 12,000 rpm and 4 °C for 30 min to isolate the supernatant for subsequent analysis. The protein concentrations of the extracted samples were accurately quantified using a BCA protein assay kit procured from Thermo Fisher, New Jersey, USA. Each sample, comprising 50 μg of protein, was meticulously prepared for the ensuing procedures. To initiate the protein processing, 10 mM dithiothreitol was added to each sample, thoroughly mixed, and allowed to incubate at 55 °C in a dry heat block for 1 h to facilitate protein denaturation and disulfide bond reduction. Subsequently, 25 mM iodoacetamide was introduced at room temperature, and the samples were incubated in darkness for 1 h to alkylate cysteine residues. Trypsin (Promega, WI, USA) was then employed for protein digestion, with an incubation period of 4 h in a 37 °C constant temperature incubator to ensure efficient peptide cleavage. After digestion, 700 μL of PBS was added to the samples, followed by an additional 12-h incubation to further digest any remaining protein fragments. Following this, 10 μL of trifluoroacetic acid was added to halt the digestion process, and desalting was performed using an OASIS HLB desalting column (Waters, USA). Finally, the desalted samples were dried using a low-temperature vacuum centrifuge to prepare them for subsequent analyses.

Peptides from per group were labeled with TMT reagent (0.8 mg powder of TMT dissolved in 41 μl acetonitrile) for 1 h at RT, and then 5 % hydroxylamine was added to incubate for 15 min at RT to terminate the reaction. The peptides were labeled with TMT labels as follows: TMT-126, hippocampus of control group; TMT-127, hippocampus of CUMS mice; TMT-128, hippocampus of XYS treated mice; TMT-129, hippocampus of FXT-treated mice. The labeled peptides from each group were mixed together, then the mixtures were desalted and dried for fractionation. The TMT labeled peptide mixture was individually fractionated using a high-pH reversed-phase peptide fractionation kit (Thermo Scientific, NJ, USA). Briefly, the peptide mixture was dissolved in 0.1 % FA and loaded onto a

fractionation column, then washed with gradually increasing concentration of acetonitrile to elute bound peptide into eight different fractions. Per fraction was dried by using vacuum centrifuge, then dissolved in 20 μl 0.1 % FA for liquid chromatography-tandem mass spectrometry (LC-MS/MS) analysis.

The peptide samples were loaded onto an Xbridge BEH300C18 chromatography column (Waters, USA) and separated using a Thermo Fisher Scientific UltiMate 3000 UHPLC system (Thermo Fisher Scientific, USA). Subsequently, the separated peptide fractions were further divided into 15 fractions according to the established protocol. Following this, all components were dried and treated with 20 μL of 0.1 % formic acid before undergoing analysis using LC-MS/MS. Finally, data analysis was performed using Proteome Discoverer software (Version 2.5, Thermo Scientific) to retrieve information from the UniProt Mouse FASTA database (released on July 20, 2023). Relative protein quantification was determined based on the ion intensity of each reported peptide, and statistical significance between any two groups was assessed using the *t*-test method in Perseus software, with the P-value threshold set to $P < 0.05$ to ensure robust statistical analysis.

2.8. Functional enrichment analysis

Screened targets underwent Gene Ontology (GO) enrichment analysis encompassing biological processes, cellular components, and molecular functions. The most significant terms, determined by their P-values, were retained to describe the functionality of the respective target modules. This analysis was conducted utilizing online resources available at http://metascape.org/. Additionally, the list of screened targets was imported into Cytoscape (Version 3.9.1) and subsequently integrated into the ClueGO plugin. The ClueGO plugin facilitated the selection of appropriate organism background and target sets from its database. A two-sided hypergeometric test was then employed to identify enriched WikiPathways or Kyoto Encyclopedia of Genes and Genomes (KEGG) signaling pathways associated with the input targets. Through this comprehensive functional enrichment analysis, deeper insights into the overarching biology of the screened targets and their potential interactions were garnered.

2.9. Molecular docking analysis

To conduct molecular docking analysis, we initially retrieved the 3D structures of protein receptors associated with the genes of interest from the AlphaFold Protein Structure Database (https://alphafold.ebi.ac.uk/) and UniProt database (https://www.uniprot.org/). Subsequently, we utilized PyMOL software to eliminate water molecules and ligands from the proteins, and then performed hydroprocessing using AutoDock Tools to ascertain the precise positioning of the active pockets. The 2D structures of the core active components were obtained from the PubChem database (https://pubchem.ncbi.nlm.nih.gov/) as ligands, which were further converted into 3D structures using ChemBio3D software. Following this step, energy optimization with MM2 was conducted. Before proceeding with the docking experiments, we assessed the affinity between protein receptors and ligands using AutoDock Vina software. A binding affinity lower than −5.0 kcal/mol indicates a favorable interaction between a protein and ligand [22]. The visualization and analysis of the docking results were then performed using the Discovery Studio 2021 client.

2.10. Western blotting

The total proteins of the samples were extracted using lysis liquid (Lot No. P0013E, Beyotime Biotech. Inc., Shanghai, China) according to the procedures laid out by the manufacturer. Subsequently, the protein concentration was determined by applying a BCA kit (Lot No. KGP902, KeyGEN BioTECH, Jiangsu, China). 10 % SDS - PAGE was used to separate the sample proteins, which were then transferred to a polyvinylidene difluoride membrane (Lot No. 1620177, Bio-Rad, Hercules, CA, USA), and TBST solution that contained 5 % milk was applied for blocking. After blocking for 1.5 h, the primary antibody was diluted with TBST solution to the following working concentrations: anti-MYDGF (myeloid cell–specific myeloid-derived growth factor, 1:1000, Proteintech, Lot No. 11353-1-AP, USA), anti-MAP4K4 (mitogen-activated protein kinase kinase 4, 1:1000, Cell Signaling Technology, Lot No. 3485 S, USA), anti-P-p65 (phosphorylation-nuclear factor NF-kappa-B p105 subunit, 1:1000, Abcam, Lot No. ab239882, England), anti-p65 (nuclear factor NF-kappa-B p105 subunit, 1:1000, Abcam, Lot No. ab32536, England), anti-P-IκBα (1:1000, Abcam, Lot No. ab133462, England), anti-IκBα (1:1000, Abcam, Lot No. ab32518, England), anti-PKC (protein kinase C, 1:1000, Abcam, Lot No. ab181558, England), anti-IL6 (1:1000, Wuhan Servicebio Technology Co., Ltd., Lot No. GB11117, China), anti-TNF-α (1:1000, Wuhan Sanying Co., Ltd., Lot No.17590-1-ap, China), and anti-β-actin (1:1000, Cell Signaling Technology, Lot No. 4967 S, USA) at 4 °C overnight. Next, the membrane was rinsed with TBST three times and incubated with a secondary antibody (1:2000, Lot No. S0001 or Lot No. S0002, Affinity Biosciences company, Jiangsu, China) for 1 h at room temperature. Finally, they were exposed using an ECL reagent kit (Thermo Science, New Jersey, USA), and the bands were visualized and analyzed using Image-Pro Plus 6.0 software (Media Cybernetics, Bethesda, USA) and normalized to the band intensities of β-actin. All experiments were repeated three times.

2.11. Statistical analysis

GraphPad PRISM (version 5.01 software) was used for all statistical analyses after first expressing them as mean ± standard deviation. One-way analysis of variance was applied to evaluate the significance of differences between each group, and the significance levels of differences found in inter-group pairwise comparisons were determined using the Student-Newman Keuls method. The results of tests with P-values <0.05 were considered to be statistically significant.

3. Results

3.1. XYS improved the bodyweight and sucrose preference percentage of CUMS-induced model mice

To evaluate the impact of XYS on depression-like symptoms, we measured the body weight and sucrose preference percentage of the CUMS model mice. Initially, no significant difference in body weight was observed among the four groups at weeks 0 and 6 ($P > 0.05$), as depicted in Fig. 1B and **C**. However, by week 12, the body weights of mice in the control, XYS, and FXT groups were significantly higher compared to those in the CUMS model group ($P < 0.001$). Similarly, there was no notable disparity in sucrose preference rate among the groups initially ($P > 0.05$, Fig. 1D and **E**). Nonetheless, at weeks 6 and 12, the sucrose preference rates of mice in the control, XYS, and FXT groups were markedly higher than those in the CUMS model group ($P < 0.001$).

3.2. XYS refined the behavioral indicators from the open field test (OFT) of CUMS-induced model mice

The OFT was employed to assess depression-like behaviors, focusing on various parameters. As illustrated in Fig. 2A–F, compared to the control group, mice in the CUMS model group exhibited significantly reduced total distance traveled, average speed, activity duration, and time spent in the central area ($P < 0.001$). Conversely, the rest time was notably prolonged in the CUMS model group compared to the control group ($P < 0.001$). Conversely, mice in the XYS and FXT groups exhibited significant reversals in the aforementioned OFT indices compared to those in the CUMS model group ($P < 0.001$).

3.3. XYS decreased serum CORT and inflammatory indices in CUMS-induced model mice

To evaluate the impact of XYS on serum CORT and inflammatory responses, including hs-CRP, NFκB, FIB, and Lp-PLA2, their serum levels were measured. As shown in Fig. 3A–E, the serum levels of CORT, hs-CRP, NFκB, FIB, and Lp-PLA2 were significantly elevated in the CUMS model group compared to the control group ($P < 0.001$). Conversely, these levels were significantly reduced in the XYS and

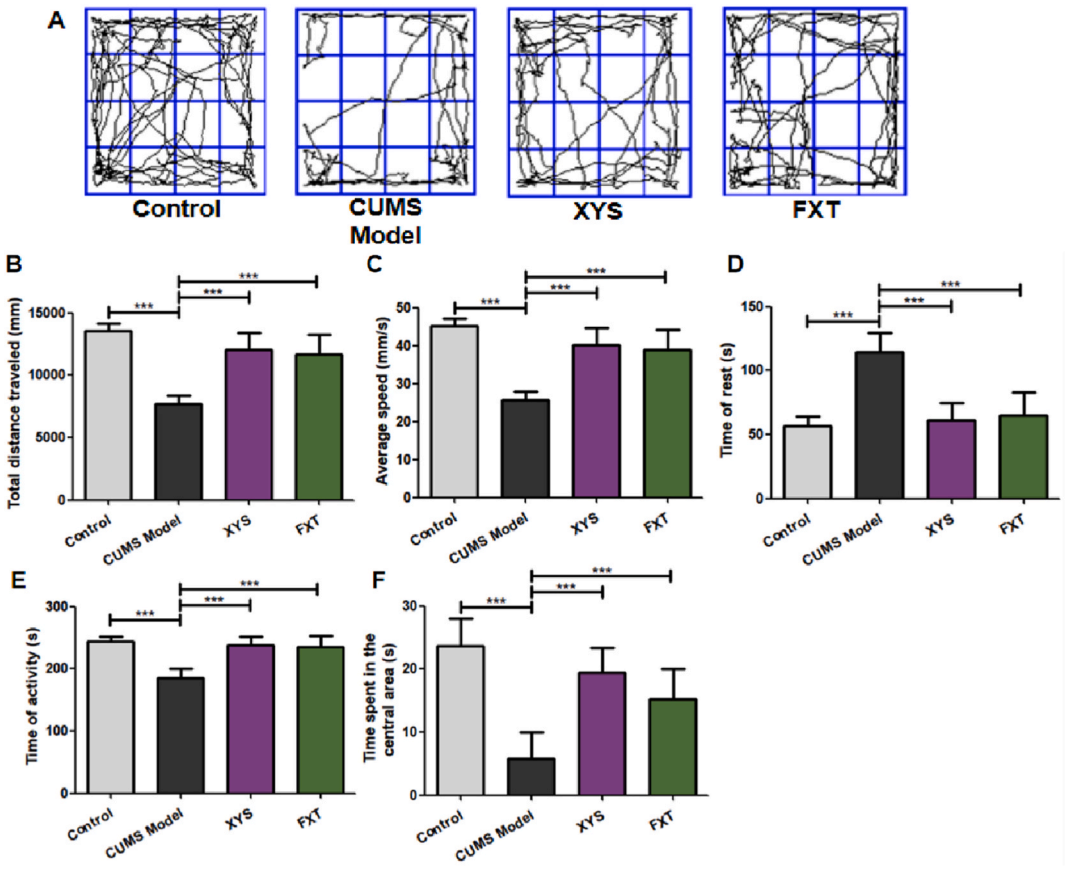

Fig. 2. Effects of XYS on open field test (OFT) of CUMS model mice. **(A)** The representative trajectory map of mice in each group in the OFT. **(B)** Bar graphs of total distance traveled in each group. **(C)** Bar graphs of average speed in each group. **(D)** Bar graphs of time of rest in each group. (E) Bar graphs of time of activity in each group. **(F)** Bar graphs of time spent in the central area in each group. n.s, *, **, and *** represent not significant, $P < 0.05$, $P < 0.01$, and $P < 0.001$ respectively, in comparison with the CUMS model group.

FXT groups compared to the control group ($P < 0.001$). Additionally, the protein expressions of IL-6 and TNF-α in the brains of mice from each group were assessed (Fig. 3F–H). The protein expressions of IL-6 and TNF-α were markedly increased in the CUMS model group compared to the control group ($P < 0.001$). However, in the XYS and FXT groups, these expressions were substantially decreased compared to the CUMS model group ($P < 0.001$).

3.4. Proteomic analysis revealed differentially expressed proteins in XYS-treated CUMS-induced model mice

To delve into the comprehensive mechanisms underlying XYS's efficacy against CUMS-induced brain injury, we conducted LC-MS-based proteomic analysis (Supplementary Table S2). $P < 0.05$ was taken as statistically significant. The increase and decrease thresholds were set at ratio ≥ 1.2 or ≤ 0.83, respectively. Initially, we identified 179 differentially expressed proteins (protein set A, Fig. 4A) between the control and CUMS model groups. Additionally, 337 (protein set B, Figs. 4B) and 386 (protein set C, Fig. 4C) differentially expressed proteins were discerned in XYS-treated mice (compared to the CUMS model group) and FXT-treated mice (compared to the CUMS model group), respectively. Moreover, 77 (protein set D, Figs. 4D) and 48 (protein set E, Fig. 4E) differentially expressed proteins were discerned in FXT-treated mice (compared to the control group) and XYS-treated mice (compared to the control group), respectively. Notably, intersecting these sets revealed 9 common proteins (MYDGF, ACTR1A, HPRT1, DNAJC11, ACIN1, MSRA, MRPS5, GSDME, and SLC1A4, Fig. 4F). Furthermore, analyzing the expression trends of these proteins across groups unveiled 7 target proteins (MYDGF, ACTR1A, HPRT1, DNAJC11, ACIN1, MSRA, and MRPS5, Fig. 4G) exhibiting significant reversal trends in the XYS and FXT groups compared to the CUMS model group.

3.5. Functional enrichment analysis provided clues to the anti-inflammation mechanism of XYS in alleviating CUMS-induced injury

The results depicted in Fig. 5A and **B** unveil a commonality of 28 proteins between protein set A and protein set B. These proteins underwent meticulous examination through signaling pathway analyses using databases like KEGG/WikiPathways and GO functional enrichment analyses, as illustrated in Fig. 5C and **D**. The enriched signaling pathways encompass a broad spectrum, including the mitogen-activated protein kinase (MAPK) signaling pathway, ribosome, spinal cord injury, Huntington's disease, Alzheimer's disease, endocytosis, RNA transport, alanine, aspartate and glutamate metabolism, and glycolysis/gluconeogenesis. Additionally, the enriched

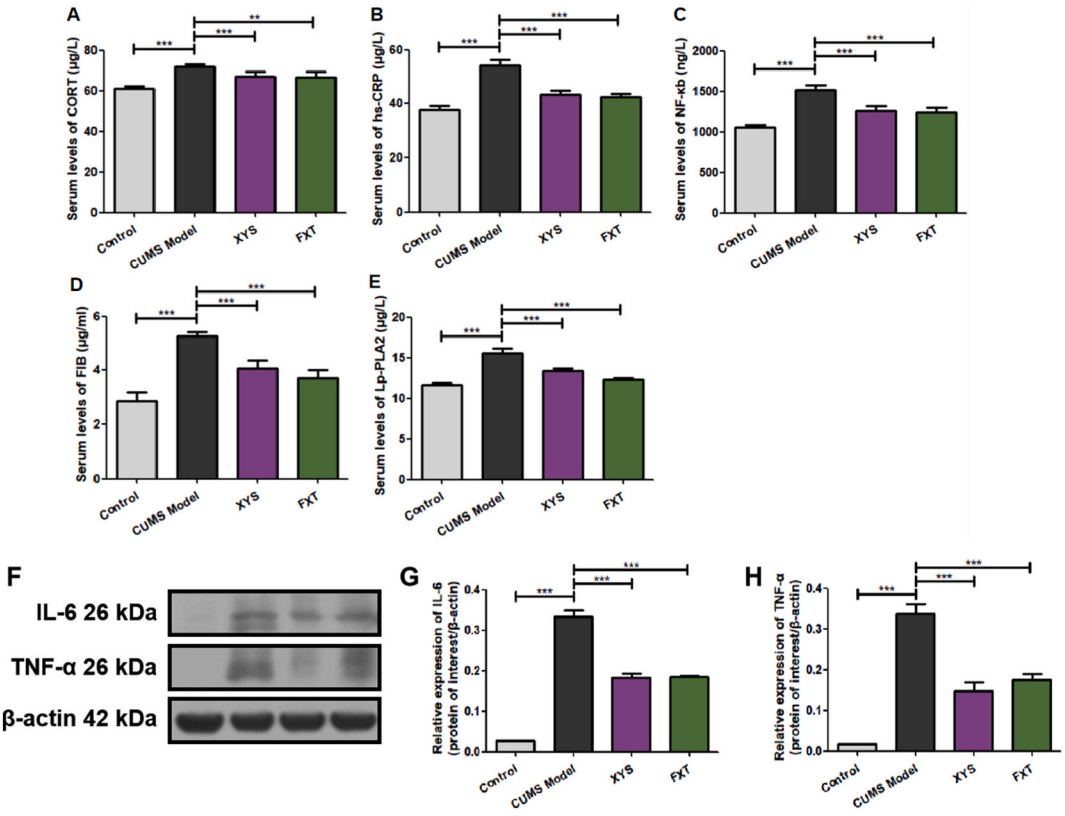

Fig. 3. Effects of XYS on inflammatory indexes of CUMS model mice. **(A)** Bar graphs of CORT in each group. **(B)** Bar graphs of hs-CRP in each group. **(C)** Bar graphs of NF-κB in each group. **(D)** Bar graphs of FIB in each group. **(E)** Bar graphs of Lp-PLA2 in each group. **(F)** Representative Western blot images of IL-6 and TNF-α. **(G)** Bar graphs of the relative expressions of IL-6 in each group. **(H)** Bar graphs of the relative expressions of TNF-α in each group. n.s, *, **, and *** represent not significant, $P < 0.05$, $P < 0.01$, and $P < 0.001$ respectively, in comparison with the CUMS model group.

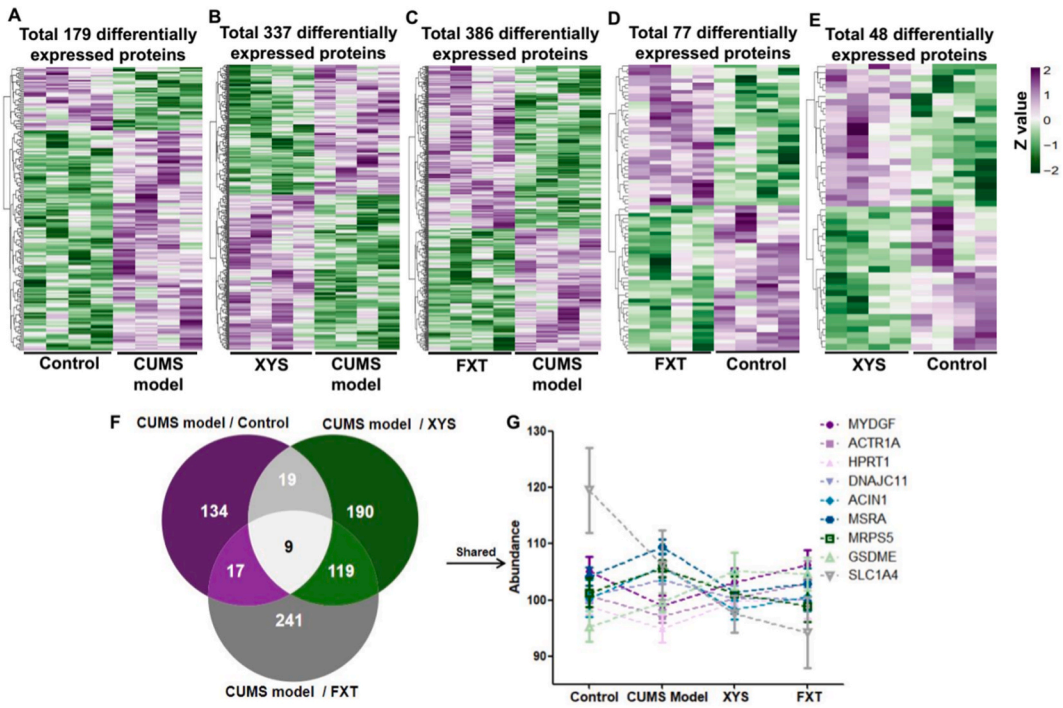

Fig. 4. The differentially expressions proteins between groups. **(A)** The 179 differentially expressions proteins between control group and CUMS model group. **(B)** The 337 differentially expressions proteins between XYS group and CUMS model group. **(C)** The 386 differentially expressions proteins between FXT group and CUMS model group. **(D)** The 77 differentially expressions proteins between FXT group and control group. **(E)** The 48 differentially expressions proteins between XYS group and control group. **(F)** The 9 intersected proteins among differentially expressions protein set A, B, and C. **(G)** The expression trends of 9 intersected proteins in each group.

GO biological processes spanned across forebrain development, brain development, telencephalon development, neuron projection development, neuron projection morphogenesis, gliogenesis, mitotic cell cycle phase transition, membrane organization, and regulation of cysteine-type endopeptidase activity. Furthermore, the GO cellular components included the neuronal cell body, dendrite, dendritic tree, and cell cortex, while the molecular functions comprised ubiquitin protein ligase binding, ubiquitin-like protein ligase binding, glycosaminoglycan binding, and molecular function inhibitor activity (Supplementary Table S3).

Moreover, the intersection of sets A and C yielded 26 proteins in common, as illustrated in Fig. 6A and **6B,** which were subjected to similar analyses, as depicted in Fig. 6C and **D**. These proteins were found to be associated with diverse signaling pathways, such as the MAPK signaling pathway, ribosome, Huntington's disease, translation factors, PPAR signaling, dopaminergic synapse, GABAergic synapse, and synaptic vesicle cycle. Additionally, they participated in various biological processes, including nucleobase-containing compound catabolic process, cellular nitrogen compound catabolic process, heterocycle catabolic process, aromatic compound catabolic process, and organic cyclic compound catabolic process. The cellular components involved centrosomes, the microtubule organizing center, the myelin sheath, and the mitochondrial protein-containing complex (Supplementary Table S3). These compelling findings underscore the potential significance of the MAPK signaling pathway in elucidating the anti-inflammatory mechanism of XYS against CUMS-induced injury.

3.6. The chemical compounds of XYS identified by UPLC-HRMS

Utilizing UPLC-HRMS to analyze typical base peaks and ion flow chromatography, we elucidated the primary active compounds present in XYS (Table 1, Fig. 7). A total of 37 primary compounds were discerned in XYS. These compounds belong to various classes, including purine nucleosides, carboxylic acids and derivatives, indoles and derivatives, prenol lipids, flavonoids, isoflavonoids, protoberberine alkaloids and derivatives, isobenzofurans, glycerophospholipids, phenols, benzene and substituted derivatives, organooxygen compounds, cinnamic acids and derivatives, fatty acyls, and linear 13 diary propanoids. Comprehensive characterizations for each compound can be found in Table 1.

3.7. Validation of the interaction between identified compounds of XYS and inflammation-related targets via molecular docking

We performed molecular docking to validate the interaction between the identified compounds of XYS and inflammation-related targets, and we observed a total of 162 pairs of "compound-targets" (87.6 % of the total), whose binding affinities were lower than −5 kcal/mol (Fig. 8A and 8B, Supplementary Table S4). As shown in Fig. 8B, the top five pairs of identified compounds with the strong

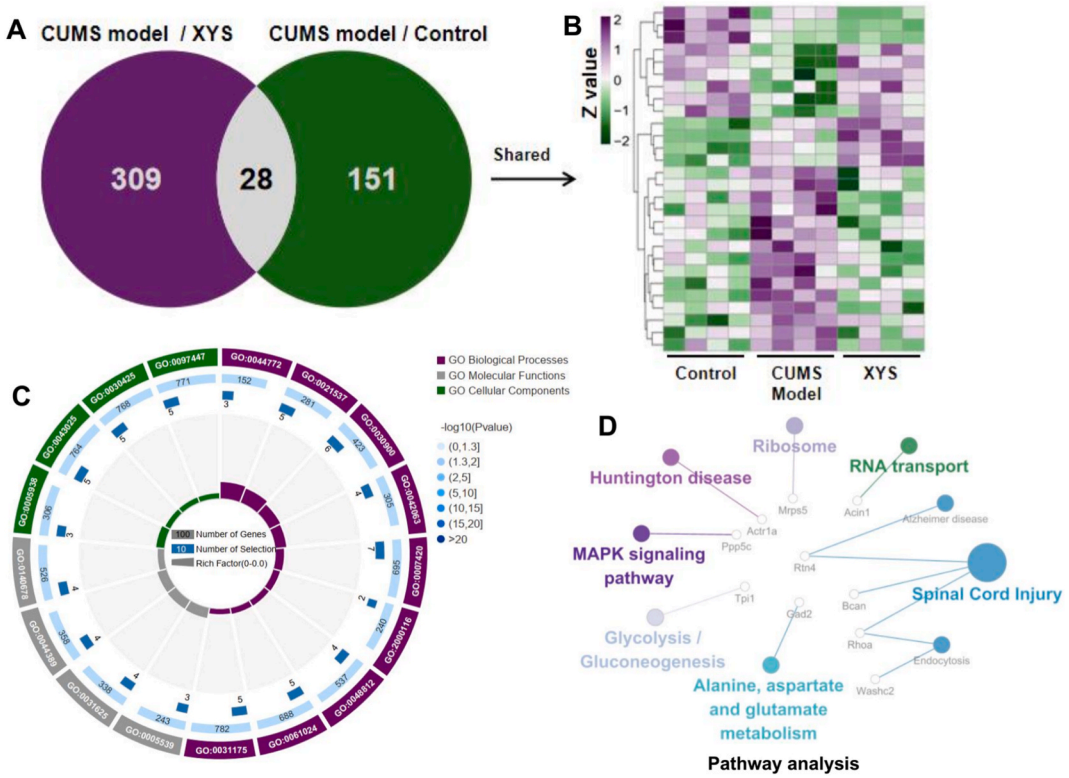

Fig. 5. Functional enrichment analysis of 28 proteins in common between differentially expression protein set A and set B. **(A)** 28 intersected proteins between differentially expression protein set A and set B. **(B)** Heatmap of differentially expression proteins among control group, CUMS model group and XYS group. **(C)** GO functional enrichment analysis of 28 intersected proteins between differentially expression protein set A and set B. **(D)** KEGG/WikiPathways enrichment analysis of 28 intersected proteins between differentially expression protein set A and set B.

binding ability and each key target were as follows: MYDGF to glycyrrhizin (−7.7 kcal/mol), diammonium glycyrrhizinate (−7.6 kcal/mol), ononin (−7.5 kcal/mol), glabrolide (−7.3 kcal/mol), and neolicuroside (−7.2 kcal/mol); PKC to diammonium glycyrrhizinate (−10.4 kcal/mol), acaciin (−10.2 kcal/mol), glycyrrhizin (−9.6 kcal/mol), Isoliquiritin (−9.3 kcal/mol), and rosmarinic acid (−9.3 kcal/mol); MAP4K4 to Glycyrrhizin (−10.6 kcal/mol), Glabrolide (−10.5 kcal/mol), diammonium glycyrrhizinate (−10.4 kcal/mol), 18.beta.-Glycyrrhetinic acid (−9.8 kcal/mol), and licoricesaponin g2 (−9.8 kcal/mol); IKBα to diammonium glycyrrhizinate (−7.9 kcal/mol), acaciin (−7.5 kcal/mol), liquiritin (−7.5 kcal/mol), glycyrrhizin (−7.4 kcal/mol), and glabrolide (−7.1 kcal/mol); p65 to glycyrrhizin (-9 kcal/mol), diammonium glycyrrhizinate (−8.9 kcal/mol), acaciin (−8.1 kcal/mol), glabrolide (−8.1 kcal/mol), and 18 beta-glycyrrhetinic acid (−7.4 kcal/mol). Fig. 8A and Table 2 present the most representative molecular docking results.

3.8. XYS inhibited the MYDGF/MAP4K4 signaling pathway in CUMS model mice

We observed that XYS could alleviate CUMS-induced injury by regulating inflammation-associated signaling pathways and the specific targets, as mentioned above, found from the bioinformatics analysis and molecular docking analysis. The protein expressions of MYDGF, PKC, MAP4K4, P-p65, p65, P-IKBα, and IKBα were measured to validate these results further. As shown in Fig. 9A–H, the relative protein expression of MYDGF decreased significantly. In contrast, the relative protein expressions of PKC, MAP4K4, P-p65, and P-IKBα were increased considerably in the CUMS model group compared to the control group ($P < 0.001$). Conversely, the expressions of these proteins were reversed significantly in the XYS and FXT groups relative to those in the CUMS model group ($P < 0.001$). There was no difference in the relative protein expressions of p65 and IKBα ($P > 0.05$) (see Fig. 10).

4. Discussion

Major depressive disorder (MDD) continues to pose a formidable challenge to global mental health, characterized not only by its high disability burden but also by its recurrent and chronic nature, which often significantly impairs an individual's quality of life. Despite decades of dedicated research, the precise etiology and pathogenesis of MDD remain elusive, owing to the intricate interplay of genetic predisposition and environmental influences [23]. Among the myriad environmental factors implicated in MDD, chronic unpredictable mild stress (CUMS) has garnered significant attention for its profound impact on neuronal structure and function, particularly within brain regions intricately involved in emotional regulation, such as the amygdala and hippocampus. This stress

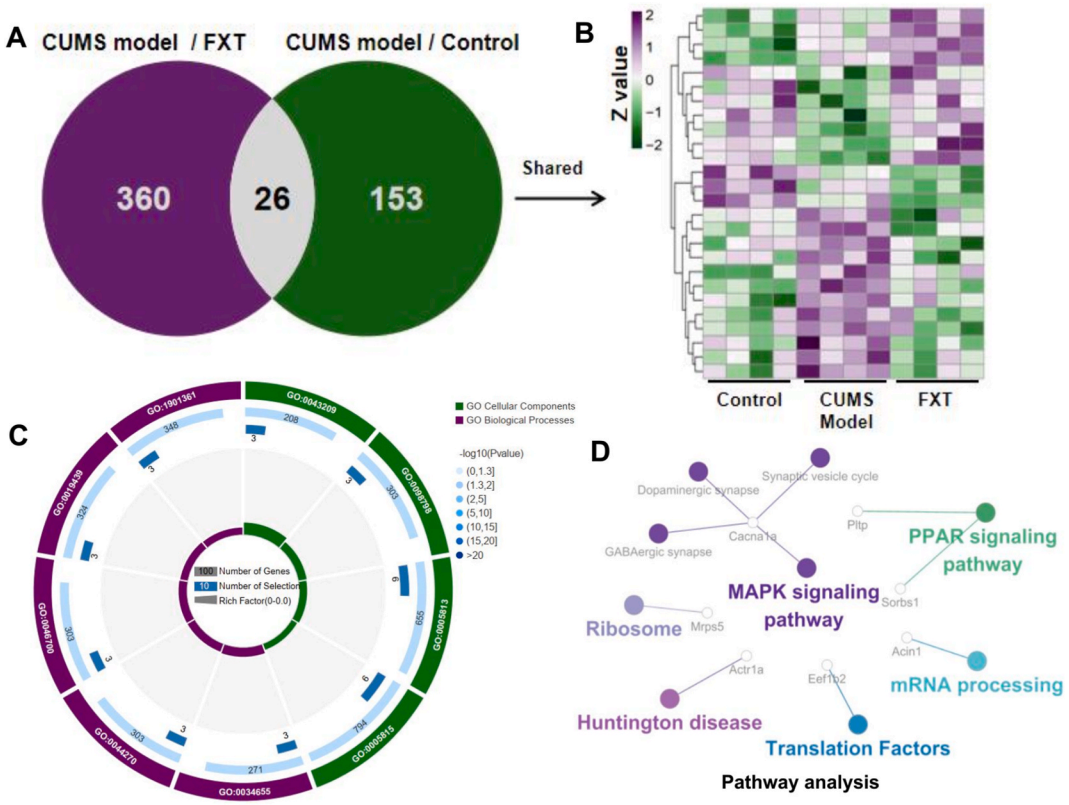

Fig. 6. Functional enrichment analysis of 26 proteins in common between differentially expression protein set A and set C. **(A)** 26 intersected proteins between differentially expression protein set A and set C. **(B)** Heatmap of differentially expression proteins among control group, CUMS model group and FXT group. **(C)** GO functional enrichment analysis of 26 intersected proteins between differentially expression protein set A and set C. **(D)** KEGG/WikiPathways enrichment analysis of 26 intersected proteins between differentially expression protein set A and set C.

paradigm, mimicking the unpredictability and chronicity of stressors encountered in daily life, serves as a reliable model for studying depressive-like behaviors and neurobiological alterations associated with MDD. Moreover, the characterization of MDD has evolved from an initially conceptualized functional disorder to a condition with well-documented structural and functional alterations in the brain, as evidenced by advancements in neuroimaging techniques [24]. These advances have shed light on aberrant neural circuitry and neurotransmitter dysregulation, providing valuable insights into the underlying neurobiology of MDD. However, the complexity of MDD necessitates a comprehensive understanding of its multifaceted etiology and pathophysiology to develop effective therapeutic interventions. In this context, traditional Chinese medicine (TCM) offers a holistic approach to addressing MDD, emphasizing the restoration of harmony and balance within the body-mind-spirit continuum. Xiaoyaosan (XYS), a classic TCM formulation with a history dating back centuries, embodies the core principles of TCM, targeting liver depression and spleen deficiency, which are often implicated in the pathogenesis of MDD [9,13–15,25,26]. Comprising a synergistic blend of herbal ingredients, each selected for its specific therapeutic properties, XYS offers a comprehensive and personalized approach to MDD treatment. For instance, Bupleuri Radix (Chaihu, CH) serves as a primary medicine in XYS, addressing liver stagnation and promoting the free flow of qi, while Angelicae Sinensis Radix (Danggui, DG) and Paeoniae Radix Alba (Baishao, BS) nourish the blood and soothe the liver, alleviating emotional disturbances. Additionally, Atractylodis Macrocephalae Rhizoma (Baizhu, BZ), Glycyrrhizae Radix Et Rhizoma (Gancao, GC), and Poria (Fuling, FL) strengthen the spleen and replenish qi, restoring vitality and resilience to stress. Furthermore, Menthae Haplocalycis Herba (Bohe, BH) and Zingiberis Rhizoma (Ganjiang, GJ) act as guiding herbs, facilitating the smooth flow of qi and harmonizing the digestive system. Together, these herbal ingredients work synergistically to rebalance the body's internal environment and alleviate the symptoms of MDD.

Pharmacological investigations have provided compelling evidence for the efficacy of XYS in ameliorating depressive-like behaviors and neurobiological alterations associated with CUMS-induced MDD. Through its multitarget and multipathway approach, XYS modulates various neurotransmitter systems, neurotrophic factors, and inflammatory mediators implicated in the pathogenesis of MDD [9,13–15,25,26]. Notably, XYS has been shown to enhance synaptic plasticity, promote neurogenesis, and attenuate neuroinflammation in preclinical models of MDD, offering a promising avenue for the development of novel antidepressant therapies. In addition to its profound effects on neurobiology, XYS exerts potent anti-inflammatory effects, which are increasingly recognized as crucial contributors to the pathophysiology of MDD [5,6]. Chronic stress-induced activation of the immune system and dysregulation of the hypothalamic-pituitary-adrenal (HPA) axis lead to sustained inflammation, contributing to neuronal damage and cognitive

Table 1
Characterization of compounds of XYS granule by UPLC-HRMS.

No.	Compound	PubChem CID	*m/z*	RT min	ppm	Adduct	Class	Score	MS/MS
1	Adenosine	447,270	268.1042	2.75	0.8	[M+H]+	Purine nucleosides	0.9915	136.06, 268.1, 119.04, 136.04, 136.08
2	Phenylalanine	6140	166.0863	3.47	18.3	[M+H]+	Carboxylic acids and derivatives	0.9997	120.08, 103.05, 166.09, 131.05, 107.05
3	L-Tryptophan	6305	205.0970	4.11	0.2	[M+H]+	Indoles and derivatives	0.997	188.07, 146.06, 118.07, 144.08, 159.09
4	L-1,2,3,4-Tetrahydro-beta-carboline-3-carboxylic acid	98,285	217.0960	4.62	14.9	[M+H]+	Indoles and derivatives	0.8207	144.08, 217.1, 74.02, 171.09, 130.07
5	Albiflorin	122173145	481.1708	5.03	1.3	[M+H]+	Prenol lipids	0.9985	105.03, 197.08, 133.06, 151.08, 105.07
6	Paeoniflorin	45358140	498.1974	5.19	0.3	[M + NH4]+	Prenol lipids	0.9992	179.07, 151.08, 133.06, 161.06, 105.07
7	Liquiritigenin	114,829	257.0801	5.61	1.3	[M+H]+	Flavonoids	0.9985	257.08,137.02,147.04,119.04,239.07
8	Isoliquiritin	5318591	419.1339	6.92	2.1	[M+H]+	Flavonoids	0.9935	257.08, 137.02, 147.04, 119.05, 239.07
9	Ononin	442,813	431.1341	7.03	0.5	[M+H]+	Isoflavonoids	0.9998	269.08, 254.06, 213.09, 237.05, 253.05
10	Acaciin	5317025	593.1871	7.44	1	[M+H]+	Flavonoids	0.9994	285.08, 447.13, 270.05, 242.06, 85.03
11	Majarine	2353	336.1234	7.67	2.1	[M+]+	Protoberberine alkaloids and derivatives	0.9987	336.12,320.09,292.09,321.09,306.07
12	Benzoylpaeoniflorin	21631106	602.2237	8.65	1.3	[M + NH4]+	Prenol lipids	0.9977	105.03,179.07,267.09,249.08,81.03
13	Glabrolide	90479675	469.3318	9.07	1.6	[M+H]+	Prenol lipids	0.9843	469.33,107.09,175.15,119.09,121.10
14	Licoricesaponin g2	14891565	839.4063	9.85	0.2	[M+H]+	Prenol lipids	0.9218	469.33,487.33,95.09,141.89,451.31
15	18.beta.-Glycyrrhetinic acid	10,114	453.3365	10.50	0.7	[M + H–H2O]+	Prenol lipids	0.9872	453.34, 107.09, 95.09, 121.1, 119.09
16	Glycyrrhizin	14,982	823.4114	11.06	1	[M+H]+	Prenol lipids	0.9981	453.33,95.09,121,10,107.09 , 454.34
17	Glycycoumarin	5317756	369.1336	11.88	1.1	[M+H]+	Isoflavonoids	0.9781	369.13, 285.08, 313.07, 270.05, 243.07
18	Ligustilide A	5319022	191.1065	13.22	1.3	[M+H]+	Isobenzofurans	0.9947	191.11, 173.1, 91.05, 145.1, 117.07
19	1-Linoleoyl-sn-glycero-3-phosphorylcholine	11988421	520.3404	13.40	0.9	[M+H]+	Glycerophospholipids	0.9189	104.11,184.07,86.10,520.34,125.00
20	[6]-Shogaol	5281794	277.1791	13.53	2.7	[M+H]+	Phenols	0.9992	137.06, 122.04, 277.22, 93.07, 79.05
21	Gallic acid	370	169.0135	3.05	3.5	[M − H]-	Benzene and substituted derivatives	0.9995	125.02, 169.01, 69.03, 97.03, 81.03
22	(R)-3-(3,4-Dihydroxyphenyl)lactate	11600642	197.0451	3.74	1.6	[M − H]-	NA	0.9955	72.99, 135.04, 123.04, 179.03, 197.05
23	3,4-Dihydroxybenzoic acid	72	153.0186	3.97	4.9	[M − H]-	Benzene and substituted derivatives	0.9995	109.03,153.02,108.02,110.03,123.04
24	3-(4-(.beta.-D-Glucopyranosyloxy)phenyl) propanoic acid	101928034	165.0550	4.47	4.5	[M-H-C6H10O5]-	Organooxygen compounds	0.9949	165.06,59.01,121.06,93.03,119.05
25	4-Formyl-2-hydroxybenzoic acid	656,876	165.0185	4.81	4.4	[M − H]-	Benzene and substituted derivatives	0.9994	121.03,165.02,122.03,93.03,77.04
26	3,4-Dihydroxyphenylacetic acid	547	167.0342	4.89	4.8	[M − H]-	Phenols	0.9992	123.04,167.03,124.05,95.05,121.03
27	Liguiritigenin-7-O-beta-D-apiosyl-4′-O-beta-D-glucoside	124578359	549.1616	5.48	0.4	[M − H]-	Flavonoids	0.9817	549.16, 255.07, 135.01, 119.05, 91.02
28	Liquiritin	503,737	417.1192	5.62	0.2	[M − H]-	Flavonoids	0.9933	255.07, 135.01, 119.05, 417.12, 91.02
29	Ferulic acid	445,858	193.0501	5.95	2.6	[M − H]-	Cinnamic acids and derivatives	0.9935	134.04,178.03,193.05,149.06,137.02
30	Rosmarinic acid	5281792	359.0774	6.53	0.5	[M − H]-	Cinnamic acids and derivatives	0.9988	161.02,197.05,133.03,135.04,73.00
31	Azelaic acid	2266	187.0970	6.65	2.7	[M − H]-	Fatty Acyls	0.9972	125.10,187.10 , 97.06,123.08,126.10
32	Salicylic acid	338	137.0235	7.14	5.7	[M − H]-	Benzene and substituted derivatives	0.998	93.03, 137.02, 94.04, 138.03, 65.04
33	Neolicuroside	6442433	255.0662	7.76	0.5	[M-H-C11H18O9]-	Flavonoids	0.9273	119.05, 255.07, 135.01, 91.02, 153.02
34	FA 18:1+3o	153,001	329.2335	9.79	6.9	[M − H]-	Fatty Acyls	0.9935	329.23,211.13,229.14,171.10,139.11
35	Isoliquiritigen	638,278	255.0661	10.13	0.9	[M − H]-	Linear 1 3 diarylpropanoids	0.9944	119.05, 255.07, 135.01, 91.02, 153.02
36	Diammonium glycyrrhizinate	77906397	821.3973	10.51	1	[M − H]-	NA	0.9854	821.4, 113.02, 71.01, 85.03, 75.01
37	4-Hydroxy-3-(3-methylbut-2-enyl)benzoic acid	443,852	205.0866	10.92	2.2	[M − H]-	Benzene and substituted derivatives	0.9245	205.09,161.10,106.04,206.09,162.10

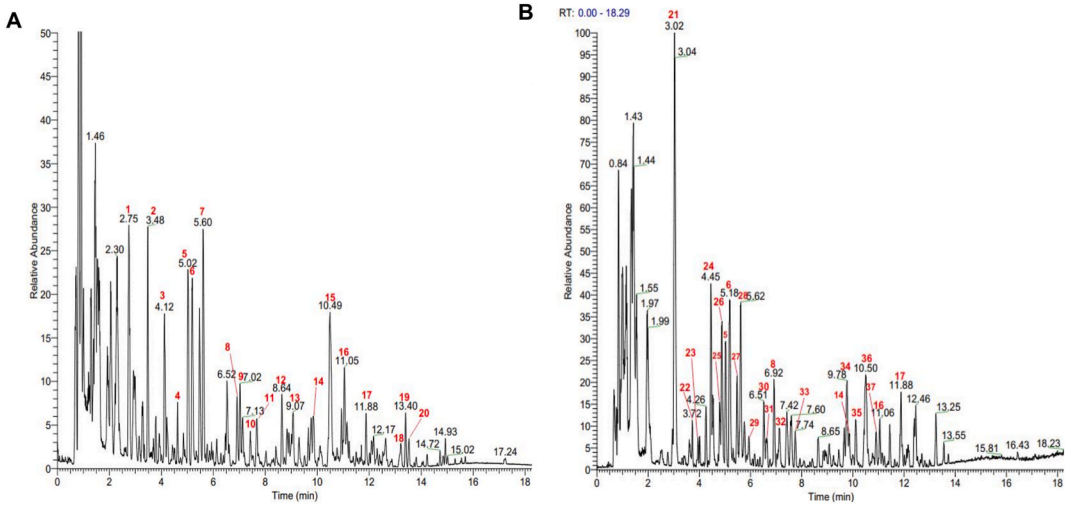

Fig. 7. Main compounds from XYS granule identified by UPLC-HRMS. **(A)** BPC diagram of XYS in positive ion mode; **(B)** BPC diagram of XYS in negative ion mode.

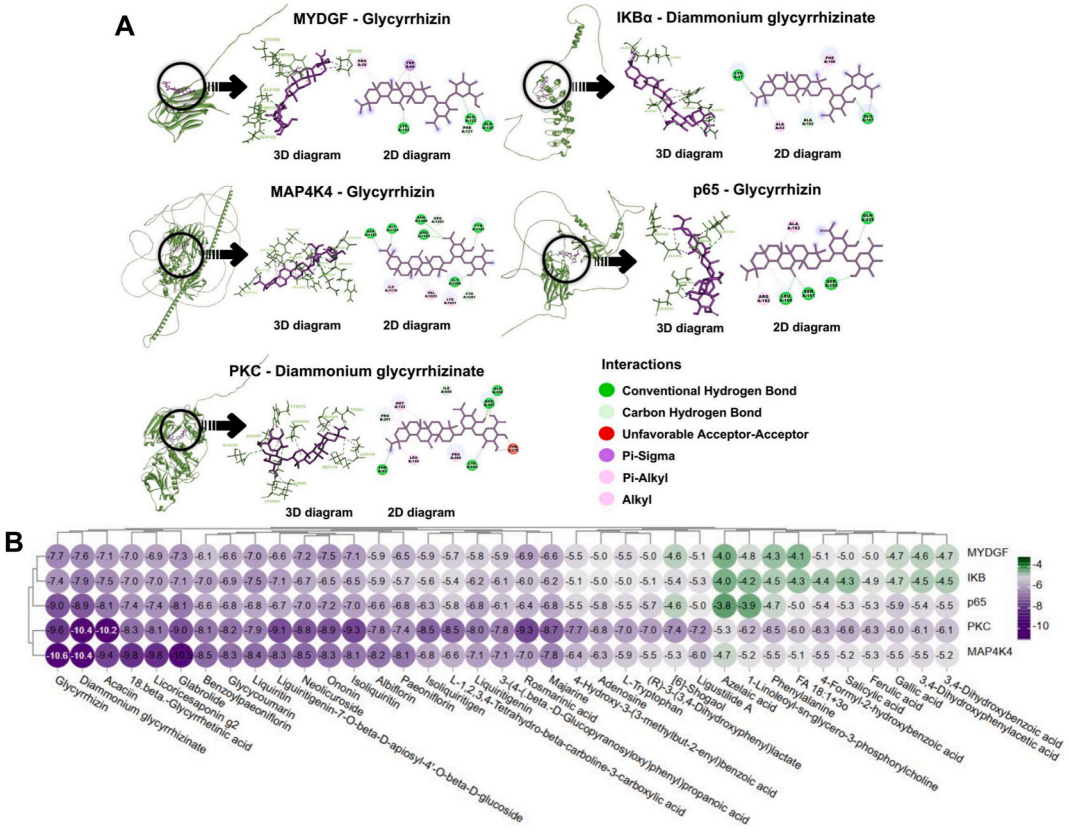

Fig. 8. Molecular docking results. **(A)** The representative docking complex of target protein and compounds. **(B)** The heatmap of docking scores of target proteins combined with 37 identified compound in XYS.

deficits observed in MDD [4]. By modulating inflammatory signaling pathways and cytokine production, XYS helps restore immune homeostasis and mitigate the detrimental effects of chronic inflammation on brain function [9,13].

The realm of proteomics represents a monumental leap forward in our comprehension of biological phenomena compared to genomics, offering a comprehensive understanding of the vast array of proteins and their functionalities within cells, tissues, or

Table 2
Representative molecular docking data of the complex of target proteins and compounds.

Target (UniProt ID)	Compound (PubChem CID)	Affinity (kcal/mol)	Conventional Hydrogen Bond	Carbon Hydrogen Bond	Unfavorable Donor-Donor	Pi-Sigma	Pi-Alkyl	Alkyl
MYDGF (Q9CPT4)	Glycyrrhizin (CID 14982)	−7.7	LYS154, GLU122, ALA120	PHE121, LYS154	–	TRP88	TRP88	PRO28
PKC (P20444)	Diammonium glycyrrhizinate (CID 77906397)	−10.4	GLU265, ASN287, THR83, LYS604	ASN287, THR83, PRO291, LE600	TYR275, ASN287	–	–	–
MAP4K4 (P97820)	Glycyrrhizin (CID 14982)	−10.6	TYR1161, GLY1202, ASP1123, GLY1124, ARG1163, ASN1204	GLY1202, TYR1161, GLY1124, CYS1201, ARG1203	–	–	–	LYS1021, VAL1023, ILE1118
IKBα (Q9Z1E3)	Diammonium glycyrrhizinate (CID 77906397)	−7.9	GLN107, LYS67	ALA102	GLN107		PHE106	ALA63, ALA102
p65 (P98152)	Glycyrrhizin (CID 14982)	−9	LEU160, SER161, GLN225, SER195	–	–	–	–	ALA193, LEU160, ARG192

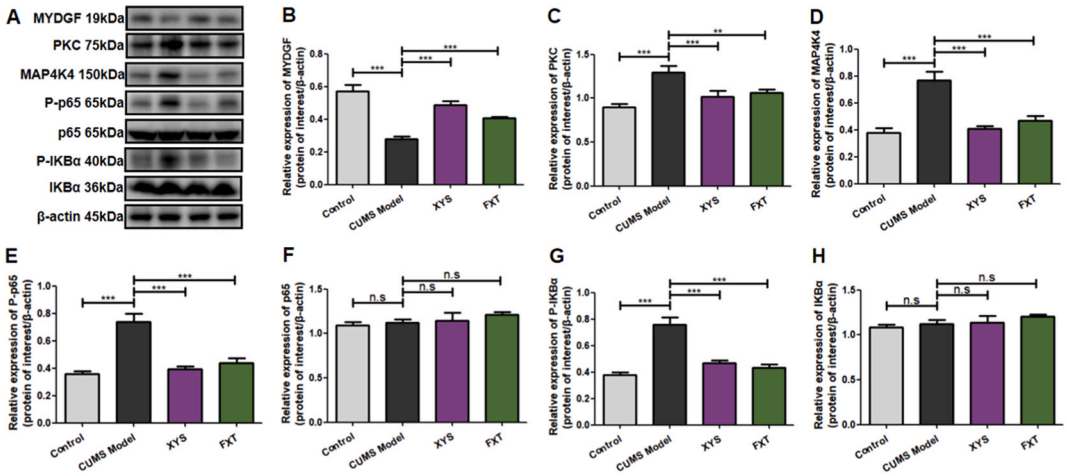

Fig. 9. Effects of XYS on MYDGF/MAP4K4/NF-κB signaling pathway of CUMS model mice. **(A)** Representative Western blot images of MYDGF, PKC, MAP4K4, P-p65, p65, P-IKBα, and IKBα. **(B–H)** Bar graphs of the relative expressions of MYDGF, PKC, MAP4K4, P-p65, p65, P-IKBα, and IKBα in each group. n.s, *, **, and *** represent not significant, $P < 0.05$, $P < 0.01$, and $P < 0.001$ respectively, in comparison with the CUMS model group.

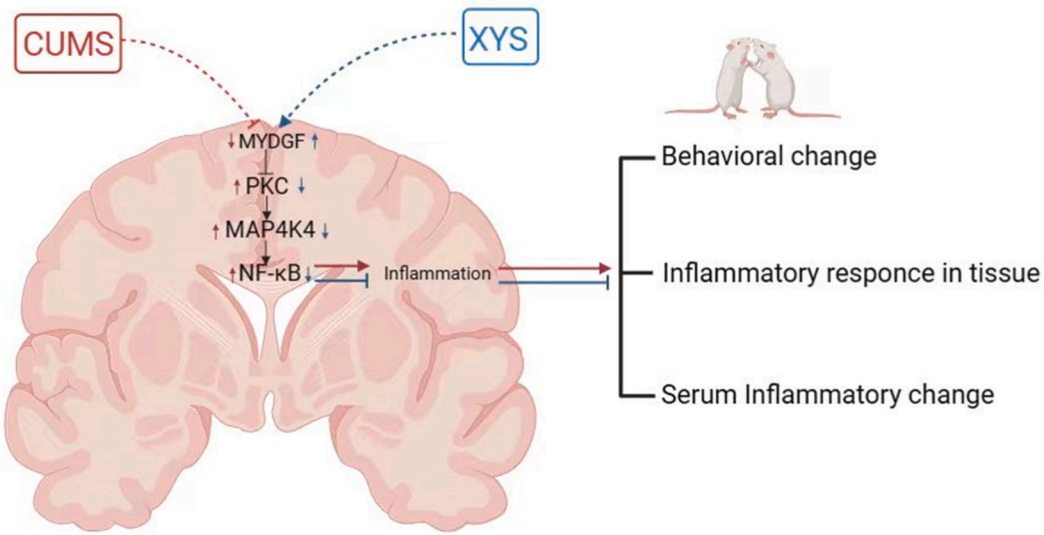

Fig. 10. Potential mechanism of the anti-inflammatory mechanism of XYS on CUMS model mice.

organisms across a myriad of processes [16–18]. Furthermore, proteomic analyses offer valuable insights into the molecular mechanisms underlying XYS's therapeutic effects, revealing alterations in protein expression profiles and signaling pathways associated with MDD pathology [15]. Through the integration of proteomic and pharmacological approaches, researchers can elucidate the complex interplay between XYS and cellular signaling networks, paving the way for the development of precision therapies for MDD. In our endeavor to delve deeper into the anti-inflammatory mechanism of XYS in mitigating CUMS-induced injury, we harnessed the power of proteomic and bioinformatics methodologies, with the aim of unraveling the intricate systemic mechanisms underlying XYS's therapeutic effects in the treatment of CUMS. Our investigation embarked on a meticulous exploration of the impact of XYS on the proteomic profiles of mouse brain tissues. This exhaustive analysis unearthed 179 differentially expressed proteins (designated as protein set A) between the control and CUMS model groups. Moreover, we identified 337 proteins (protein set B) and 386 proteins (protein set C) exhibiting differential expression in XYS-treated mice (relative to the CUMS model group) and fluoxetine (FXT)-treated mice (relative to the CUMS model group), respectively. Notably, among these, seven target proteins (MYDGF, ACTR1A, HPRT1, DNAJC11, ACIN1, MSRA, and MRPS5) displayed conspicuous reversal trends in the XYS and FXT groups compared to the CUMS model group. The proteomic results reflected that XYS and FXT could affect specific protein expression in brain tissue through specific molecular mechanisms, which might involve multiple signaling pathways and biological processes related to CUMS. On the one hand, XYS and FXT could not only improve the known mechanisms and targets of CUMS. On the other hand, XYS might also act on other

unknown targets and signaling pathways, and further experiments are needed to verify whether these unknown signaling pathways are related to the treatment of CUMS.

From the experimental results, both XYS and FXT could improve the behavioral and inflammatory indicators of the CUMS model. An intriguing convergences of 28 proteins (XYS) was observed between protein sets A and B, meanwhile, the intersection of protein sets A and C yielded 26 proteins (FXT), prompting subsequent signaling pathway and gene ontology (GO) functional enrichment analyses. According to the functional enrichment analysis results, there were similarities and differences between XYS and FXT in biological processes (BP), cellular components (CC), and molecular functions (MF) and signaling pathways. Regarding the signaling pathway, XYS and FXT share the following similarities: MAPK signaling pathway, Huntington disease, and Ribosome. Additionally, the enriched pathway terms of FXT included mRNA processing, Translation Factors, PPAR signaling pathway, Dopaminergic synapse, GABAergic synapse, and Synaptic vesicle cycle; the pathway enriched terms of XYS included Spinal Cord Injury, Alzheimer disease, Endocytosis, RNA transport, Alanine, aspartate and glutamate metabolism, and Glycolysis/Gluconeogenesis. Regarding BP, CC, and MF, there are the following differences between FXT and XYS: The enriched BP terms of FXT included nucleobase-containing compound catabolic process, cellular nitrogen compound catabolic process, and heterocycle catabolic process; The enriched CC terms of FXT comprised centrosome, microtubule organizing center, myelin sheath, and mitochondrial protein-containing complex. The enriched BP terms of XYS included forebrain development, brain development, telencephalon development, and neuron projection development; The enriched CC terms of XYS composed of neuronal cell body, Dendrite, dendritic tree, and cell cortex; The enriched MF terms of XYS comprised ubiquitin protein ligase binding, ubiquitin-like protein ligase binding, glycosaminoglycan binding, and molecular function inhibitor activity. It has been known that the pharmacological mechanism of FXT in treating MDD is primarily based on its regulation of the neurotransmitter 5-hydroxytryptamine (5-HT, also known as serotonin). FXT is a selective serotonin reuptake inhibitor (SSRI) that selectively inhibits the 5-HT transporter, blocking the reuptake of 5-HT by the presynaptic membrane, thus prolonging and increasing the duration of 5-HT's action in the synaptic cleft. However, the underlying pharmacological mechanism of FXT on MDD involved in anti-inflammation remains unclear. A prior research found that the anti-MDD effects of FXT partially profited from neuroprotection against inflammation and neuronal apoptosis via downregulation of the p38 MAPK pathway, which is consistent with our findings in this study [27]. In addition, another study demonstrated that FXT could alleviate post-traumatic stress disorder via promoting autophagy and inhibiting neuroinflammation [28]. According to the retrieval references from databases, there has been no relevant research on MYDGF mediated pathway in the treatment of MDD with FXT or XYS yet.

The application of proteomics applied in this study provided an advanced perspective for exploring the inflammatory pathological mechanisms of MDD. What caught our attention the most from the present study was the differential expression of MYDGF in the XYS-treated group. Because there have been few reports about MYDGF in the pathogenesis and therapy of MDD or CUMS-induced injury yet. Despite the absence of MYDGF in the field of MDD, MYDGF played an important role in the pathogenesis of other diseases. It has already been shown that MYDGF can attenuate vascular inflammation and alleviate atherosclerosis through MAP4K4/NF-κB signaling. Thus, MYDGF may be a critical inflammation-regulating factor in the development of atherosclerosis [29]. Moreover, overexpression of MYDGF inhibits apoptosis, oxidative stress, and cytokine secretion of gingival fibroblasts induced by high glucose levels by suppressing the NF-κB pathway [30], and MYDGF can also alleviate nonalcoholic fatty liver disease and inflammation in a manner involving IKKβ/NF-κB signaling. MYDGF also contributes to the crosstalk between the liver and bone marrow [31]. Existing evidence points towards MYDGF's involvement in regulating inflammation across various contexts, thereby underscoring its potential as a therapeutic target of XYS in the treatment of CUMS. MYDGF emerged as a key player in our investigation, albeit its role in MDD pathogenesis remaining relatively underexplored. We therefore propose that the anti-inflammatory mechanism of XYS in treating CUMS is strongly associated with the MYDGF/MAP4K4/NF-κB signaling pathway.

Expanding upon these insightful findings, we emphasized the paramount role of the MYDGF/MAP4K4/NF-κB signaling pathway in orchestrating the inflammatory response in mice, thereby shedding illuminating light on XYS's anti-inflammatory mechanism in ameliorating CUMS-induced injury. The molecular docking assays lent further credence to our findings by validating the interaction between the active compounds of XYS and potential targets. It was observed that there were a total of 162 pairs of "compound-targets" (87.6 % of the total), whose binding affinities were lower than −5 kcal/mol (Fig. 8A and B, Supplementary Table S4). The top five pairs of identified compounds with the strong binding ability and each key target were as follows: MYDGF to glycyrrhizin, diammonium glycyrrhizinate, ononin, glabrolide, and neolicuroside; PKC to diammonium glycyrrhizinate, acaciin, glycyrrhizin, Isoliquiritin, and rosmarinic acid; MAP4K4 to Glycyrrhizin, Glabrolide, diammonium glycyrrhizinate, 18.beta.-Glycyrrhetinic acid, and licoricesaponin g2; IKBα to diammonium glycyrrhizinate, acaciin, liquiritin, glycyrrhizin, and glabrolide; p65 to glycyrrhizin, diammonium glycyrrhizinate, acaciin, glabrolide, and 18 beta-glycyrrhetinic acid. With noteworthy compounds such as glycyrrhizin and diammonium glycyrrhizinate exhibited robust affinity for inflammatory-associated proteins. Previous randomized placebo-controlled clinical trial confirmed that glycyrrhizin could effectively alleviate the MDD and down-regulate the inflammatory indexes [32]. *In vivo* experiment demonstrated that glycyrrhizin could restrain HMGB1 thus improving chronic stress-induced depressive behavior through regulating kynurenine pathway [33]. Another study showed that glycyrrhizin prevents TauO-induced senescence through inhibition of MAPK and NF-κB the essential signaling pathways for inflammatory senescence-associated secretory phenotype development [34]. Preceding research revealed that diammonium glycyrrhizinate could inhibit Aβ-induced inflammation *in vitro* and *in vivo* by suppressing the activation of MAPK and NF-κB signaling pathways [35]. An additional study also proved that diammonium glycyrrhizinate had a protective effect on cerebral ischemia-reperfusion injury and neuroinflammation in rats by decreasing caspase-3, p38 MAPK and MMP-9 [36]. Further validation through western blotting analysis corroborated these intricate findings, revealing that XYS exerted significant modulation on the expression of key proteins involved in inflammation. The pivotal role of the MAPK pathway in both the pathogenesis and therapy of major depressive disorder (MDD) is increasingly recognized, with mounting evidence implicating its dysregulation in depression-related brain regions. Notably, our study underscores the potential therapeutic significance of targeting

the MAPK pathway to alleviate MDD.

Looking towards the horizon, future directions may encompass identifying the active compounds of XYS through ultra-high-performance liquid chromatography coupled with high-resolution mass spectrometry (UPLC-HRMS) analysis of drug-containing serum, delving deeper into the anti-inflammatory effects of compounds such as glycyrrhizin and diammonium glycyrrhizinate, and conducting *in vitro* experiments to dissect the mechanistic underpinnings of XYS in CUMS-induced injury. In summary, XYS exerts its anti-inflammatory effects in CUMS model mice through the modulation of the MYDGF/MAP4K4/NF-κB signaling pathway, offering promising avenues for future research and therapeutic development. The contributions of proteomics to our understanding of biological processes cannot be overstated. As Pandey and Mann [37] astutely observed, proteomics offers invaluable insights into the functional activities of proteins that genomics alone cannot provide. Similarly, Zang et al. [38] elucidated the superiority of proteomic analyses in capturing the dynamic nature of biological activities. Thus, our study underscores the profound significance of proteomic approaches in unraveling the intricate mechanisms underlying the therapeutic effects of traditional Chinese medicine formulations like XYS in addressing multifactorial disorders such as MDD.

Funding

This study is supported by the National Natural Science Foundation of China (No. 82104746); Guangdong Basic and Applied Basic Research Foundation (No. 2022A1515011647, No. 2021A1515110706); Shenzhen Science and Technology Program (No. JCYJ20230807094603007); Shenzhen Municipal Scheme for Basic Research (No. JCYJ20210324100208022); Key Basic Research Program of Shenzhen Science and Technology Innovation Commission (No. JCYJ20200109150717745); Guangzhou Science and Technology Program (No. 202201011643); Scientific research project of traditional Chinese Medicine Bureau of Guangdong Province (No. 20221354); Shenzhen Traditional Chinese Medicine Hospital “3030 Program" Chinese Medicine Clinical Research Project (No. G3030202133).

Ethics statement

Animal experiments were conducted adhering to the ARRIVE guidelines and with approval from the Local Ethical Committee (Guangzhou University of Chinese Medicine, Approval No. 20200817009, Date 17th Augst 2020).

Data availability statement

The data that has been used is confidential.

CRediT authorship contribution statement

Ruolan Huang: Writing – review & editing, Supervision, Resources, Project administration, Investigation, Funding acquisition, Conceptualization. **Shenglan Gong:** Validation, Project administration, Methodology, Investigation, Formal analysis, Data curation. **Bocheng Xiong:** Visualization, Validation, Software, Methodology, Data curation. **Xifei Yang:** Visualization, Validation, Methodology, Investigation, Data curation. **Chongyang Chen:** Visualization, Validation, Software, Methodology, Investigation, Formal analysis, Data curation. **Wei Song:** Validation, Software, Resources, Methodology, Investigation, Formal analysis, Data curation. **Ruodai Wu:** Investigation, Formal analysis, Data curation. **Li Yang:** Software, Investigation, Formal analysis, Data curation. **Jia Yin:** Writing – review & editing, Supervision, Project administration, Conceptualization. **Mingtai Chen:** Writing – review & editing, Writing – original draft, Funding acquisition, Conceptualization.

Declaration of competing interest

We the undersigned declare that this manuscript entitled “A classic famous prescription alleviates inflammation in CUMS model mice via modulating MYDGF/MAP4K4/NF-κB signaling pathway, verified through UPLC-HRMS and proteomics analysis” is original, has not been published before and is not currently being considered for publication elsewhere. We would like to draw the attention of the Editor to the following publications of one or more of us that refer to aspects of the manuscript presently being submitted. Where relevant copies of such publications are attached.

We confirm that the manuscript has been read and approved by all named authors (Ruolan Huang, Shenglan Gong, Bocheng Xiong, Xifei Yang, Chongyang Chen, Wei Song, Ruodai Wu, Li Yang, Jia Yin, Mingtai Chen). We further confirm that the order of authors listed in the manuscript has been approved by all of us. The authors declare that they have no conflicts of interest.

We understand that the Corresponding Author is the sole contact for the Editorial process. He/she is responsible for communicating with the other authors about progress, submissions of revisions and final approval of proofs.

Acknowledgements

We would like to appreciate the entire research team for their collective efforts and contributions to this project. The authors thank AiMi Academic Services (www.aimieditor.com) for English language editing and review services.

Appendix A. Supplementary data

Supplementary data to this article can be found online at https://doi.org/10.1016/j.heliyon.2024.e34596.

References

[1] A.I. Campos, et al., Brain correlates of suicide Attempt in 18,925 Participants across 18 International Cohorts, Biol Psychiatry 90 (4) (2021) 243–252.
[2] R. Barnett, Depression, Lancet 393 (10186) (2019) 2113.
[3] V.L. Ruberto, M.K. Jha, J.W. Murrough, Pharmacological treatments for patients with treatment-Resistant depression, Pharmaceuticals 13 (6) (2020).
[4] A. Cattaneo, et al., Candidate genes expression profile associated with antidepressants response in the GENDEP study: differentiating between baseline 'predictors' and longitudinal 'targets', Neuropsychopharmacology 38 (3) (2013) 377–385.
[5] B.E. Leonard, Inflammation and depression: a causal or coincidental link to the pathophysiology? Acta Neuropsychiatr. 30 (1) (2018) 1–16.
[6] A.H. Miller, V. Maletic, C.L. Raison, Inflammation and its discontents: the role of cytokines in the pathophysiology of major depression, Biol Psychiatry 65 (9) (2009) 732–741.
[7] C.A. Köhler, et al., Peripheral cytokine and chemokine alterations in depression: a meta-analysis of 82 studies, Acta Psychiatr. Scand. 135 (5) (2017) 373–387.
[8] O. Kohler, et al., Inflammation in depression and the potential for anti-inflammatory treatment, Curr. Neuropharmacol. 14 (7) (2016) 732–742.
[9] M. Chen, et al., Xiaoyaosan (Tiaogan-Liqi therapy) protects peritoneal macrophages from corticosterone-induced stress by regulating the interaction between glucocorticoid receptor and ABCA1, Ann. Transl. Med. 8 (22) (2020) 1506.
[10] M. Chen, et al., Effects of Xinkeshu tablets on coronary heart disease patients combined with anxiety and depression symptoms after percutaneous coronary intervention: a meta-analysis, Phytomedicine 104 (2022) 154243.
[11] M. Chen, et al., Effectiveness and safety of modified 'Huoxue Shugan' formulas on coronary heart disease combined with depression: protocol for a systematic review, BMJ Open 8 (11) (2018) e022868.
[12] J. Hu, et al., Clinical efficacy and safety of traditional Chinese medicine Xiao Yao San in insomnia combined with anxiety, Medicine (Baltim.) 100 (43) (2021) e27608.
[13] Z.Y. Yan, et al., Antidepressant mechanism of traditional Chinese medicine formula Xiaoyaosan in CUMS-induced depressed mouse model via RIPK1-RIPK3-MLKL mediated necroptosis based on network pharmacology analysis, Front. Pharmacol. 12 (2021) 773562.
[14] J. Zeng, et al., Xiaoyaosan ethyl acetate fraction alleviates depression-like behaviors in CUMS mice by promoting hippocampal neurogenesis via modulating the IGF-1Rβ/PI3K/Akt signaling pathway, J. Ethnopharmacol. 288 (2022) 115005.
[15] X. Zhu, et al., Xiaoyaosan ameliorates chronic restraint stress-induced depression-like phenotype by suppressing A2AR signaling in the rat Striatum, Front. Pharmacol. 13 (2022) 897436.
[16] M.R. Wilkins, et al., Progress with proteome projects: why all proteins expressed by a genome should be identified and how to do it, Biotechnol. Genet. Eng. Rev. 13 (1996) 19–50.
[17] X. Li, W. Wang, J. Chen, Recent progress in mass spectrometry proteomics for biomedical research, Sci. China Life Sci. 60 (10) (2017) 1093–1113.
[18] Z.Y. Zhang He, Prospect the application of systems biology in traditional Chinese medicine research, China Journal of Traditional Chinese Medicine and Pharmacy 35 (1) (2020) 31–35.
[19] M. Chen, et al., A classical herbal formula alleviates high-fat diet induced nonalcoholic steatohepatitis (NASH) via targeting mitophagy to rehabilitate dysfunctional mitochondria, validated by UPLC-HRMS identification combined with in vivo experiment, Biomed. Pharmacother. 168 (2023) 115831.
[20] M. Chen, et al., Integrating network analysis and experimental validation to reveal the mitophagy-associated mechanism of Yiqi Huoxue (YQHX) prescription in the treatment of myocardial ischemia/reperfusion injury, Pharmacol. Res. 189 (2023) 106682.
[21] S. Yu, et al., Xiao-Yao-San reduces blood-brain barrier injury induced by chronic stress in vitro and vivo via glucocorticoid receptor-mediated upregulation of Occludin, J. Ethnopharmacol. 246 (2020) 112165.
[22] K.Y. Hsin, S. Ghosh, H. Kitano, Combining machine learning systems and multiple docking simulation packages to improve docking prediction reliability for network pharmacology, PLoS One 8 (12) (2013) e83922.
[23] T.P. Bittar, B. Labonté, Functional contribution of the medial Prefrontal circuitry in major depressive disorder and stress-induced depressive-like behaviors, Front. Behav. Neurosci. 15 (2021) 699592.
[24] M.T. Davis, et al., Acute cognitive effects of single-dose intravenous ketamine in major depressive and posttraumatic stress disorder, Transl. Psychiatry 11 (1) (2021) 205.
[25] M. Chen, et al., Investigating the mechanisms of Modified Xiaoyaosan (tiaogan-liqi prescription) in suppressing the progression of atherosclerosis, by means of integrative pharmacology and experimental validation, Aging (Albany NY) 13 (8) (2021) 11411–11432.
[26] M. Chen, et al., Traditional Chinese medicine in the treatment of nonalcoholic steatohepatitis, Pharmacol. Res. 172 (2021) 105849.
[27] Y. Zhao, et al., Neuroprotective effects of fluoxetine against chronic stress-induced neural inflammation and apoptosis: involvement of the p38 activity, Front. Physiol. 11 (2020) 351.
[28] C. Lou, et al., Fluoxetine protects against inflammation and promotes autophagy in mice model of post-traumatic stress disorder, Behav. Brain Res. 433 (2022) 114004.
[29] B. Meng, et al., Myeloid-derived growth factor inhibits inflammation and alleviates endothelial injury and atherosclerosis in mice, Sci. Adv. 7 (21) (2021).
[30] L. Gao, et al., Myeloid-derived growth factor regulates high glucose-mediated apoptosis of gingival fibroblasts and induce AKT pathway activation and nuclear factor κB pathway inhibition, J. Dent. Sci. 18 (2) (2023) 636–644.
[31] Y. Ding, et al., Myeloid-derived growth factor alleviates non-alcoholic fatty liver disease alleviates in a manner involving IKKβ/NF-κB signaling, Cell Death Dis. 14 (6) (2023) 376.
[32] Z.Y. Cao, et al., Glycyrrhizic acid as an adjunctive treatment for depression through anti-inflammation: a randomized placebo-controlled clinical trial, J. Affect. Disord. 265 (2020) 247–254.
[33] B. Wang, et al., Glycyrrhizic acid ameliorates the kynurenine pathway in association with its antidepressant effect, Behav. Brain Res. 353 (2018) 250–257.
[34] S. Gaikwad, et al., Tau oligomer induced HMGB1 release contributes to cellular senescence and neuropathology linked to Alzheimer's disease and frontotemporal dementia, Cell Rep. 36 (3) (2021) 109419.
[35] H. Zhao, et al., Diammonium glycyrrhizinate attenuates Aβ(1-42) -induced neuroinflammation and regulates MAPK and NF-κB pathways in vitro and in vivo, CNS Neurosci. Ther. 19 (2) (2013) 117–124.
[36] H. Wang, et al., Effect of diammonium glycyrrhizinate in improving focal cerebral ischemia-reperfusion injury in rats through multiple mechanisms, Dose Response 20 (4) (2022) 15593258221142792.
[37] A. Pandey, M. Mann, Proteomics to study genes and genomes, Nature 405 (6788) (2000) 837–846.
[38] T. Zang, et al., The biochemistry of blister fluid from pediatric burn injuries: proteomics and metabolomics aspects, Expert Rev. Proteomics 13 (1) (2016) 35–53.